SUPPLEMENTARY INFORMATION

SUPPLEMENTAL FIGURE LEGENDS

Supplemental figure 1. hGFAP-cre-mediated recombination in the developing and postnatal brain.

(A) The lineage relationship between neural stem cells, progenitor cells, and differentiated cells is illustrated. The hGFAP-cre transgene is expressed in radial glia during embryonic development, and in type B neural stem cells as well as mature astrocytes in the postnatal brain (all three hGFAP-cre-expressing cell types are marked by dashed lines). Of note, mouse GFAP (mGFAP) is not expressed in radial glia. This genetic targeting system permits to introduce a mutation into diverse brain cell populations including those that do not express hGFAP-cre (e.g. SVZ-derived neuroblasts, $NG2^{+}$ glial progenitors, oligodendrocytes and neurons). (B) Brain sections from hGFAP-cre+;R26R-LacZ double transgenic mice at ages of postnatal day 0.5 (P0.5, upper panels) and P21 (lower panels) were stained with X-gal and imaged at three different magnifications. By neonate stages, hGFAP-cre-mediated recombination evidenced by β-gal expression has already extensively occurred in the dorsal forebrain. (C) Brain sections from adult hGFAP-cre+;R26R-LacZ double transgenic mice were stained with anti-β-gal/anti-Olig2 (a, a'), anti-β-gal/anti-GFAP (b, b'), and anti-GFAP/anti-Cre (c, c'). Most of β-gal-positive cells in the corpus callosum express Olig2 (arrows, a'), indicating that these cells are glial progenitors or oligodendrocytes. Consistently, the majority of GFAP-positive cells in the corpus callosum do not express β-gal (arrows, b'), despite their expression of hGFAP-cre transgene (arrows, c'). These observations are consistent with the previous reports that the R26R-LacZ does not efficiently report Cre-mediated recombination in most mature astrocytes in the forebrain. Of note, GFAP-expressing cells in the SVZ can readily be marked by β-gal (arrowheads, b') and these cells also express hGFAP-cre (arrowheads, c'). Ctx, cerebral cortex; OB, olfactory bulb; Hp, hippocampus; LV and "*", lateral ventricle. Scale bar, 100 μm.

Supplemental figure 2. Histopathology of high-grade $p53^{\Delta E5\text{-}6}$ malignant astrocytic gliomas.

(A) Sections from two representative Grade III malignant astrocytic gliomas (GIII 1, 2) were

stained with hematoxylin and eosin (H&E) (a, a'), anti-GFAP (b, b'), anti-Nestin (c, c'), and anti-Olig2 (d, d'). The arrows in (a-d) point to the lateral ventricle. (B) High-magnification views of (A) illustrate a high degree of heterogeneity in lineage marker expression within individual tumor and between tumors. Arrows in (B) point to mitotic figures in tumors, the diagnostic feature of high-grade gliomas in humans. Scale bar, 50 μm.

Supplemental figure 3. Expression of PDGFRα in $p53^{\Delta E5-6}$ malignant astrocytic gliomas.

Cryostat sections from an early-stage glioma (A, D, G, J), a Grade III glioma (B, E, H, K), and a GBM (C, F, I, L) were stained with H&E (A-C) and anti-PDGFRα (D-F). The dashed lines in (A-F) roughly mark the border of the tumors and surrounding brain tissues. Compared to normal brain tissues that have low or no PDGFRα expression, malignant gliomas at all stages exhibit high levels of PDGFRα expression. It is worth noting that regardless of presence or absence of necrosis, $p53^{\Delta E5-6}$ glioma cells similarly exhibit a high degree of nuclear atypia (G-I), suggesting that this model resembles primary GBM. LV, lateral ventricle; Ctx, cerebral cortex; OB, olfactory bulb. (G, H, I) and (J, K, L) show the high-magnification views of the tumors in (A, B, C) and (D, E, F), respectively. Scale bar, 100 μm.

Supplemental figure 4. Expression of CD133 in normal brain and malignant astrocytic gliomas.

(A) Sections of normal brain (a) and three representative gliomas (b, c, d) were stained with anti-CD133 (red) and DAPI (blue). (a' to d') High magnification views of (a to d) illustrates that a subpopulation of glioma cells express CD133 (b, c, d) whereas only ependymal cells in the normal brain were immunoreactive for CD133 (a). Arrowheads in (b, d) point to $CD133^{+}$ malignant glioma cells, many of which were identified around the blood vessels (BV, d, d'). The dashed lines in (b) mark the border of the tumor and normal brain tissues. Ctx, cerebral cortex; Hp, hippocampus; LV or "*", lateral ventricle. (B) Serial sections from a GBM with focal areas containing a significant number of $CD133^{+}$ cells were stained with anti-CD133/anti-p53 (a), anti-CD133/anti-Nestin (b), anti-CD133/anti-Olig2 (c), and anti-CD133/anti-CD31 antibodies (d). These sections were counterstained with DAPI for labeling tumor nuclei (a' to d'). Arrows in (d)

show $CD133^+/CD31^-$ tumor cells and arrowheads point to a minor population of $CD133^+/CD31^+$ endothelial cells that surround the blood vessels (*) in the tumor. Scale bar, 50 μm.

Supplemental figure 5. Comparison of control and $p53^{\Delta E5-6}$ mutant brains at 2 months of age.
The brains of control and mutant mice at age of 2 months were sagittally sectioned, and stained with H&E (A, B and D, E) or anti-BrdU (C, F). Two independent positions (~ 100 μm apart) at sagittal planes along the midline to lateral hemisphere were selected to compare the size and cellular density of the SVZ between control and mutant brains. (G, H, I) and (J, K, L) show the high-magnification views of the SVZ areas in (A, B, C) and (D, E, F), respectively. No significant difference in cell density and proliferation was identified between control and mutant SVZ. LV, lateral ventricle. (M) Quantification of the number of the SVZ cells; (N) the density of the SVZ cells that was presented by the number of SVZ cells per unit length of the LV; (O) the number of BrdU-positive cells in the SVZ and corpus callosum (CC), $p = 0.52$ (SVZa), $p = 0.61$ (SVZp), $p = 0.81$ (CC); and (P) the density and (Q) percentage of the BrdU-positive cells in the SVZ between control and mutant brains. Data were presented by mean ± SEM. $p < 0.05$ is considered as statistically significant. No detectable abnormality was identified in mutant brains of $p53^{\Delta E5-6}$ mice at 2 months of age. Scale bar, 100 μm.

Supplemental figure 6. Analysis of the PI3K/Akt signaling pathway in malignant gliomas from CKO1, CKO2 and CKO3 mice.
The brains with high-grade malignant gliomas from $p53^{\Delta E5-6}$ (CKO1/2) (A-L) and $p53^{\Delta E5-6}$;$Nf1^{-/-}$ (CKO3) (M-R) mice were sectioned and stained with an anti-p-Akt antibody, which labels the cells with activated PI3K/Akt signaling pathway. Based upon the number and pattern of p-Akt-positive cells, the $p53^{\Delta E5-6}$ gliomas are highly heterogeneous and can be classified into three types: (1) Type 1 tumors have very extensive p-Akt staining and typically have 40 to 60% of p-Akt-positive cells (A-F), (2) Type 2 tumors only have a small number of p-Akt-positive cells (G-I), and (3) Type 3 tumors exhibit no p-Akt staining (J-L). In contrast, the $p53^{\Delta E5-6}$;$Nf1^{-/-}$ gliomas are relatively homogeneous and uniformly exhibit extensive and intense p-Akt staining (M-R). The images in each row were taken at three different magnifications from independent glioma

samples. The dashed lines in (A, D, G, J, M, and P) roughly demarcate the border of the tumors and surrounding brain tissues. Ctx, cerebral cortex; "*", lateral ventricle. Scale bar, 100 μm.

Suppemantal figure 7. High-grade malignant gliomas in $p53^{\Delta E5-6}$;$Nf1^{-/-}$ mice exhibit relatively homogeneous histological features.

Sections from a representative Grade III glioma (A-H) and a GBM (I-P) of $p53^{\Delta E5-6}$;$Nf1^{-/-}$ (CKO3) mice were stained with H&E (A and E, I and M), anti-GFAP (B and F, J and N), anti-Nestin (C and G, K and O), and anti-Olig2 (D and H, L and P). The CKO3 malignant gliomas exhibit relatively homogeneous expression pattern of lineage markers as compared to CKO1/2 tumors. The dashed lines in (A-D) and (I-L) mark the border of tumors and normal brain tissues. N, necrosis. Scale bar, 100 μm.

Supplemental figure 8. Continuous expansion of the $p53^{\Delta E5-6}$-positive cells underlies glioma development.

The images taken at two magnifications (A, B) show $p53^{\Delta E5-6}$-positive glioma cells from one representative $p53^{\Delta E5-6}$ mutant brain in the early stages of tumor development. The dashed lines in (A, B) mark the $p53^{\Delta E5-6}$-positive early lesion. (C) Adjacent sections of the mutant brain with this early lesion (A, B) were stained with anti-p53 (a, e, i), anti-Ki67 (b, f, j), anti-Nestin (c, g, k), and anti-Olig2 (d, h, l). Arrows in (a to d) mark the length of the RMS in these images. RMS, rostral migratory stream; Ctx, cerebral cortex; CC, corpus callosum. "*" marks lateral ventricle. (e, i), (f, j), (g, k), and (h, l) are the high-magnification views of the boxed areas marked in (a), (b), (c), and (d), respectively. Scale bar, 100 μm.

Supplemental figure 9. Lineage marker expression of $p53^{\Delta E5-6}$-positive glioma precursors in the corpus callosum and SVZ.

This figure shows the high-magnification views of the images shown in Figure 7C, which has a proliferating cluster involving both the corpus callosum and SVZ. Arrows and arrowheads in (A to E) point to morphologically similar $p53^{\Delta E5-6}$-positive glioma precursors in the corpus callosum and SVZ, respectively. These proliferating $p53^{\Delta E5-6}$-positive glioma precursors exhibit the lineage marker expression pattern of $Nestin^{+}/Olig2^{+}/GFAP^{-}/PSA\text{-}NCAM^{-}$, resembling SVZ-C*

transit-amplifying progenitors. The dashed lines mark the SVZ. LV, lateral ventricle. Scale bar, 50 μm.

Supplemental table 1. Negative controls for p53 immunohistochemical analysis.
Sections of normal brains from mice with genotypes of hGFAP-cre-;$p53^{flox/KO}$, hGFAP-cre;$p53^{flox/flox}$, hGFAP-cre-;$p53^{flox/flox}$;$Nf1^{KO/+}$, and hGFAP-cre+;$p53^{flox/+}$ were stained with an anti-p53 antibody. In addition, mutant brains containing GBMs from Mut1 and Mut3 (hGFAP-cre+;$p53^{KO/KO}$;$Nf1^{flox/flox}$ and hGFAP-cre+;$p53^{KO/+}$;$Nf1^{flox/+}$) (Zhu et al., 2005) were sectioned and stained with an anti-p53 antibody. No p53 staining was detected in these normal brains or GBMs with a p53-null mutation. These results indicate that the detectable level of mutant $p53^{\Delta E5\text{-}6}$ expression is highly specific to the $p53^{\Delta E5\text{-}6}$ brain tumor cells. N values indicate the number of the mice used for these experiments.

Supplemental table 2. Summary of immunohistochemical analysis of malignant astrocytic gliomas from CKO1, CKO2 and CKO3 mice.
Compared to the highly heterogeneous $p53^{\Delta E5\text{-}6}$ gliomas (CKO1 and CKO2), the CKO3 gliomas exhibit relatively homogeneous expression pattern in lineage markers and consistent activation of MAPK and PI3K/Akt signaling pathways. For example, the $p53^{\Delta E5\text{-}6}$;$Nf1^{-/-}$ gliomas typically exhibited low or moderate levels of GFAP expression, intense and widespread Nestin expression, and almost universally high levels of Olig2 expression. Notably, high levels of GFAP expression were only observed in the $p53^{\Delta E5\text{-}6}$ glioma cells, but never in $p53^{\Delta E5\text{-}6}$;$Nf1^{-/-}$ gliomas.

Supplemental table 3. The location and number of $p53^{\Delta E5\text{-}6}$-positive cells in the early stages of glioma development.
The brains of $p53^{\Delta E5\text{-}6}$ mutant mice at ages of 6 to 9 months were serially sectioned at sagittal planes and stained with an anti-p53 antibody. The number and distribution of $p53^{\Delta E5\text{-}6}$-positive cells were identified under a light microscope. We designed a scheme to classify the early-stage gliomas into four stages based upon the number and absence/presence of $p53^{\Delta E5\text{-}6}$-positive cell clusters. Specifically, Stage 0 (N) contains no $p53^{\Delta E5\text{-}6}$-positive cells; Stage 1 (S1) contains fewer than 10 $p53^{\Delta E5\text{-}6}$-positive cells in the specific brain areas; Stage 2 (S2) contains 10 to 50 $p53^{\Delta E5\text{-}6}$-

positive cells without forming cell clusters; and Stage 3 (S3) has $p53^{\Delta E5-6}$-positive cell clusters with more than 50 cells. Fourteen of 15 mutant brains (14/15) without microscopically visible tumors were serially sectioned and prepared for 5-μm paraffin sections. P53 immunohistochemical staining reveals that all of the 14 mutant brains analyzed contained $p53^{\Delta E5-6}$-positive cells in the areas of the corpus callosum that is immediately adjacent to the SVZ or RMS. In contrast, only 2 of these 14 brains had additional $p53^{\Delta E5-6}$-positive cells in the areas that are not directly linked to the SVZ or RMS (e.g. OB). SVZa, anterior subventricular zone (SVZ); RMS, rostral migratory stream; CC, corpus callosum; Ctx, cerebral cortex. ND, not determined.

EXPERIMENTAL PROCEDURES (Detailed methods)

RT-PCR analysis and sequencing of the $p53^{\Delta E5-6}$ allele.

Total RNAs were isolated from 7 $p53^{\Delta E5-6}$ brain tumors, 2 hGFAP-cre+;$p53^{-/-}$;$Nf1^{flox/flox}$ GBMs (Zhu et al., 2005), and 2 $Smad3^{-/-}$ colon cancers (Zhu et al., 1998), and were used to synthesize cDNAs by using the SuperScript system (Invitrogen). The following primers were designed to analyze various parts of the p53 coding region (5' to 3'):

P1, AGGTAGCGACTACAGTTAGGGG; P2, TGAAGTCATAAGACAGCAAGGAG;
P3, CCTGCCATCACCTCAC; P4, GGAAGCCATAGTTGCC;
P5, TCTGTTATGTGCACGTACTC; P6, CGGGTGGCTCATAAGG;
P7, GCCGGCTCTGAGTATA; P8, TGTGATGATGGTAAGGA.

The p53 normal and mutant transcripts, encoding the entire open reading frame, was amplified with primers 1 and 2, purified, and sequenced. In some experiments, the p53 mutant transcripts were also subcloned into the TA Cloning Vector (Invitrogen) and 1 to 4 independent clones were used for sequencing. For some tumors, the sequences of the p53 coding region were further analyzed by using genomic DNAs.

Histology and tumor analysis

Mice were aged until signs of distress appeared. Then, mice were perfused with 4% paraformaldehyde (PFA) and brains were dissected, followed by overnight post-fixation in 4% PFA at 4 ºC. Brains were divided into two hemispheres along the midline and each hemisphere was processed for either paraffin-embedded or cryostat sections. Serial sections were sagittally prepared at 5 μm for paraffin sections or 14 μm for cryostat sections. Every eleventh slide was stained by H&E. Stained sections were independently examined under a light microscope by Y.Z. and P.E.M. Tumor grading was determined by Y.Z. and P.E.M. based upon the WHO grading system for malignant astrocytic glioma and medulloblastoma (Louis et al., 2007). Adjacent sections were subjected to immunohistochemical analysis (see below). For PCR analysis, tumor tissues and tails were dissected in ice-cold PBS, digested with proteinase K, and genotyped as described (Lin et al., 2004).

Histological grading of malignant astrocytic gliomas in CKO1, CKO2 and CKO3 mice

Histopathology of neoplasms that developed in these mice had to meet diagnostic criteria of the World Health Organization (WHO) for classification of tumors of the CNS (Louis et al., 2007). Tumors with neoplastic astrocytes were classified as astrocytic gliomas. Astrocytic features include extension of cellular processes from neoplastic cells. These vary from long and thick to thin and short. They are highlighted with H&E and GFAP stains. Variable nuclear shapes, particularly elongated, bent and dark staining nuclei characterize neoplastic astrocytes. Their perinuclear cytoplasm is highly variable: from imperceptible to substantial and appearing to push the nucleus to the perimeter of the cell. Astrocytic glioma is a classification that includes astrocytoma, anaplastic astrocytoma, glioblastoma, and oligoastrocytoma. To be among the first three tumors, neoplastic astrocytes must predominate. To be either an anaplastic astrocytoma (WHO grade III on a scale of four) or glioblastoma (WHO grade V), the tumor must have mitoses. It must be crowded with malignant cells, cells with coarse nuclear chromatin, angulated and pleomorphic nuclei, or nucleolar abnormalities. To be classified as a glioblastoma and given the highest grade of malignancy, the additional feature of either necrosis or microvascular proliferation must be present. Microvascular proliferation is hypotrophy and hyperplasia of cells in the walls of tumor vessels.

LacZ/β-gal staining

The R26R-LacZ transgene was introduced to the CKO1 and CKO2 mice. Mice with genotypes of hGFAP-cre+;$p53^{flox/KO}$;R26R-LacZ+ (CKO1) and hGFAP-cre+;$p53^{flox/flox}$;R26R-LacZ+ (CKO2) were generated. Brains were collected from mutant mice at ages of postnatal day (P0.5), P21, and 6 months. Tumor tissues were isolated from mutant mice with high-grade brain tumors. Dissected tissues were post-fixed in PFA for 2 hours and transferred to 30% sucrose for overnight dehydration. Frozen sections cut at 10 μm were prepared and subjected to X-gal staining for 1 hour to overnight depending on the signal intensity. X-gal stained sections were then subjected to nuclear fast red for counterstaining. Co-localization of β-gal expressing cells with other lineage markers was obtained by double immunofluorescence.

Western Blot analysis

Snap-frozen tissues from normal brains and tumors were homogenized in 1X SDS loading buffer [50 mM Tris-HCL (pH6.8), 2% SDS, 0.05% bromophenol blue, 10% glycerol, 100mM β-mercaptoethanol]. Samples were analyzed by SDS-PAGE and transferred onto PVDF membranes (Millipore). The blots were then blocked in 5% non-fat milk in TBST, followed by incubation of primary antibodies at 4°C overnight. After washing, the blots were incubated in horseradish peroxidase (HRP)-conjugated secondary antibodies at room temperature for 1 hour. Signals were detected using ECL or ECL plus (GE healthcare) followed by film development. The primary antibodies used are as follows: p-Akt (1:1000, Cell Signaling), Akt (1:1000, Cell Signaling), p-Erk (1:1000, Cell Signaling), Erk (1:1000, Cell Signaling), PDGFRα (1:500, eBiosciences), PDGF-A (1:200, Santa Cruz), PDGF-B (1:200, Santa Cruz), Pten (1:1000, Cell Signaling), *Nf1* (1:1000, Santa Cruz), Cdk4 (1:2000, Santa Cruz), Cyclin D1 (1:200, Santa Cruz), p16 (1:200, Santa Cruz), Rb (1:1000, Santa Cruz), p21 (1:1000, BD), p27 (1:2000, BD), β-actin (1:10000, Sigma).

Immunohistochemistry/ Immunofluorescence

Paraffin sections were deparaffinized and rehydrated. Sections were subjected to immunohistochemical analysis as described previously (Zhu et al., 1998; Zhu et al., 2001). The visualization of primary antibodies was performed with either a horseradish peroxidase system using a diaminobenzidine-based (DAB) peroxidase substrate (Vectastain ABC kit, Vector) or immunofluorescence by using Cy2 (or Alexa 488)-conjugated and Cy3 (or Alexa 555)-conjugated secondary antibodies at 1:200 dilution (Cy2/Cy3, Jackson Immunoresearch; Alexa 488/555, Invitrogen). The dilutions of primary antibodies used in this study were: p53 (1:500, rabbit, Novo Castra), BrdU (1:1000, rat, Abcam), Ki-67 (1:500, mouse, BD Pharmingen), CD133 (1:500, rat, eBiosciences), PDGFRα (1:1000, rat, eBiosciences), Olig2 (Rabbit, 1:20000, a kind gift from Dr. C. Stiles; guinea pig, 1:10000, a kind gift from Dr. B. Novitch), GFAP (1:2000, mouse, BD Pharmingen), MAP2 (1:200, mouse, Sigma), Nestin (1:100, mouse, Chemicon), PSA-NCAM (1:1000, mouse, Chemicon), NG2 (1:200, mouse, Millipore),), β-gal (1:1000, rabbit, 5 prime and 3 prime) , β-gal (1:1000, goat, AbD Serotec), and CD31 (1:200, mouse, Dako). CD133 or PDGFRα staining was performed on cryostat sections, and an

Invitrogen biotin/streptavidin system was used for signal amplification. Sections were examined under either a light or a fluorescence microscope (Olympus).

BrdU Assay

The CKO1/CKO2 mutant and control littermates were pulsed with BrdU five times a day at 2-hour intervals. The dose of BrdU was 50 μg/g (gram, body weight). Mice were perfused with 4% PFA 2 hours after the last pulse. Brains were dissected and processed for either paraffin-embedded or cryostat sections. BrdU immunohistochemical analysis was performed as described previously (Zhu et al., 1998).

REFERENCES

Lin, S. C., Lee, K. F., Nikitin, A. Y., Hilsenbeck, S. G., Cardiff, R. D., Li, A., Kang, K. W., Frank, S. A., Lee, W. H., and Lee, E. Y. (2004). Somatic mutation of p53 leads to estrogen receptor alpha-positive and -negative mouse mammary tumors with high frequency of metastasis. Cancer Res *64*, 3525-3532.

Louis, D. N., Ohgaki, H., Wiestler, O. D., and Cavenee, W. K. (2007). WHO Classification of Tumors of the Central Nervous System, (Lyon IARC).

Zhu, Y., Guignard, F., Zhao, D., Liu, L., Burns, D. K., Mason, R. P., Messing, A., and Parada, L. F. (2005). Early inactivation of p53 tumor suppressor gene cooperating with NF1 loss induces malignant astrocytoma. Cancer Cell *8*, 119-130.

Zhu, Y., Richardson, J. A., Parada, L. F., and Graff, J. M. (1998). Smad3 mutant mice develop metastatic colorectal cancer. Cell *94*, 703-714.

Zhu, Y., Romero, M. I., Ghosh, P., Ye, Z., Charnay, P., Rushing, E. J., Marth, J. D., and Parada, L. F. (2001). Ablation of NF1 function in neurons induces abnormal development of cerebral cortex and reactive gliosis in the brain. Genes Dev *15*, 859-876.

Supplemental Figure 1

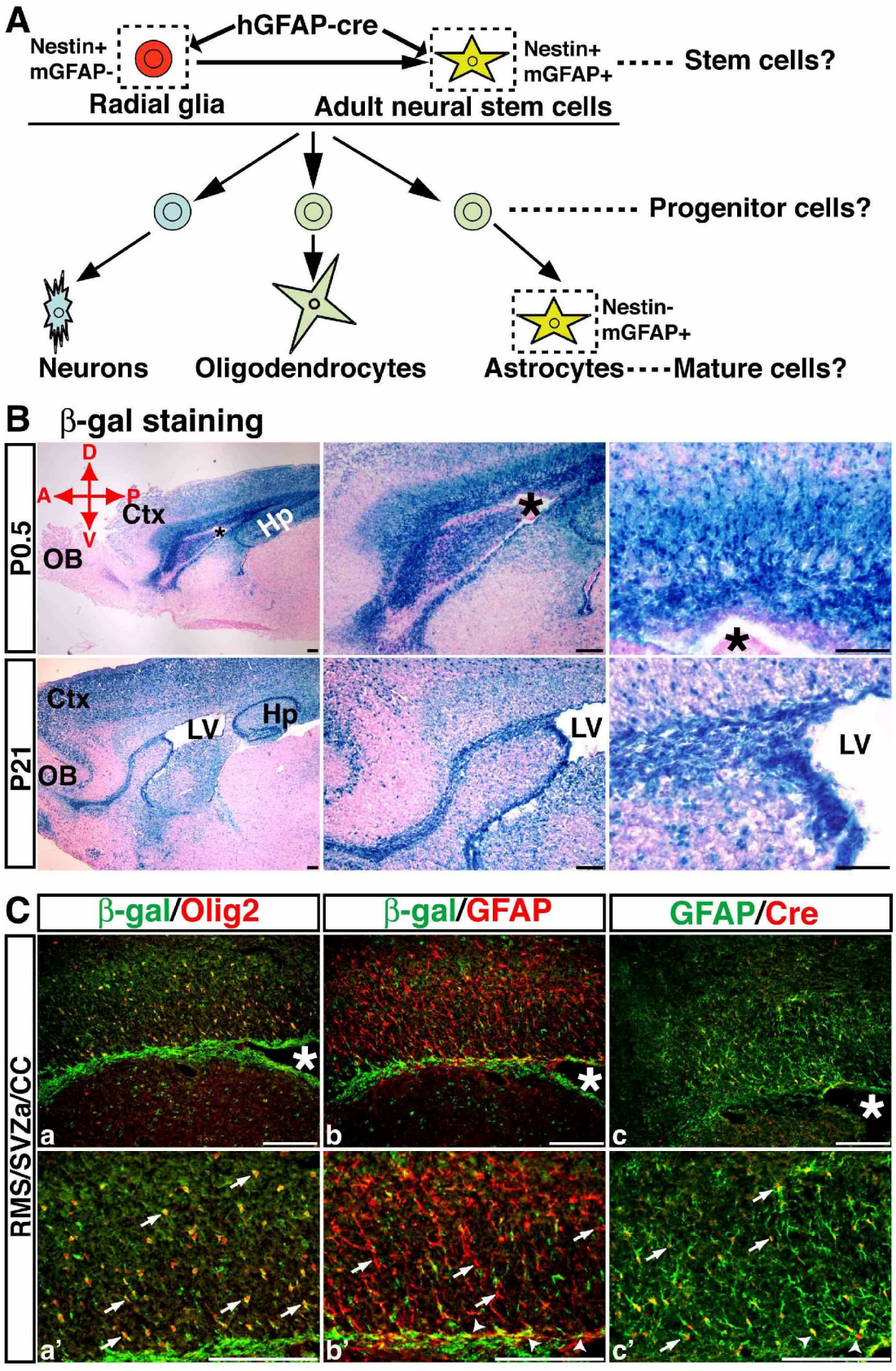

Supplemental Figure 2

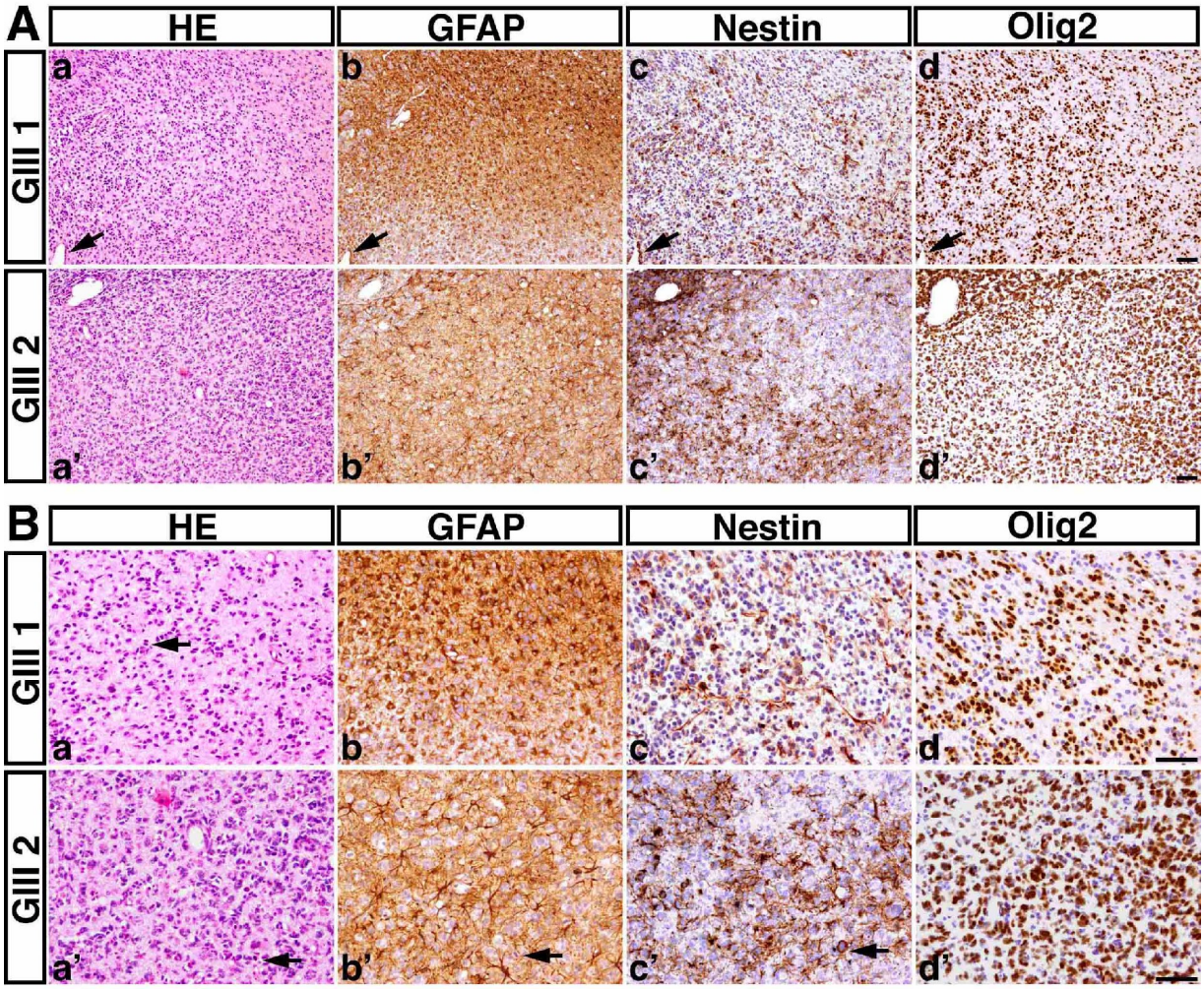

Supplemental Figure 3

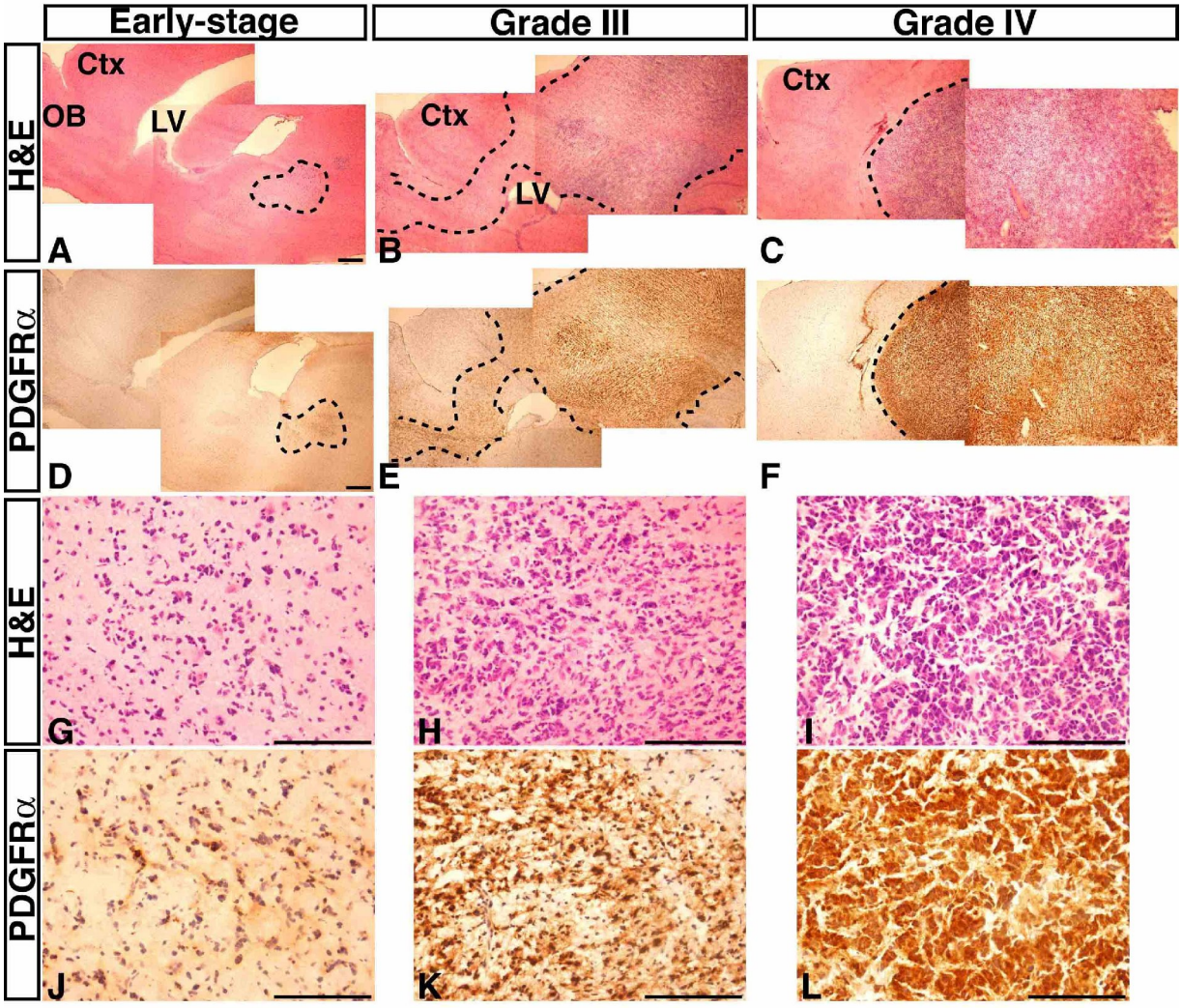

Supplemental Figure 4

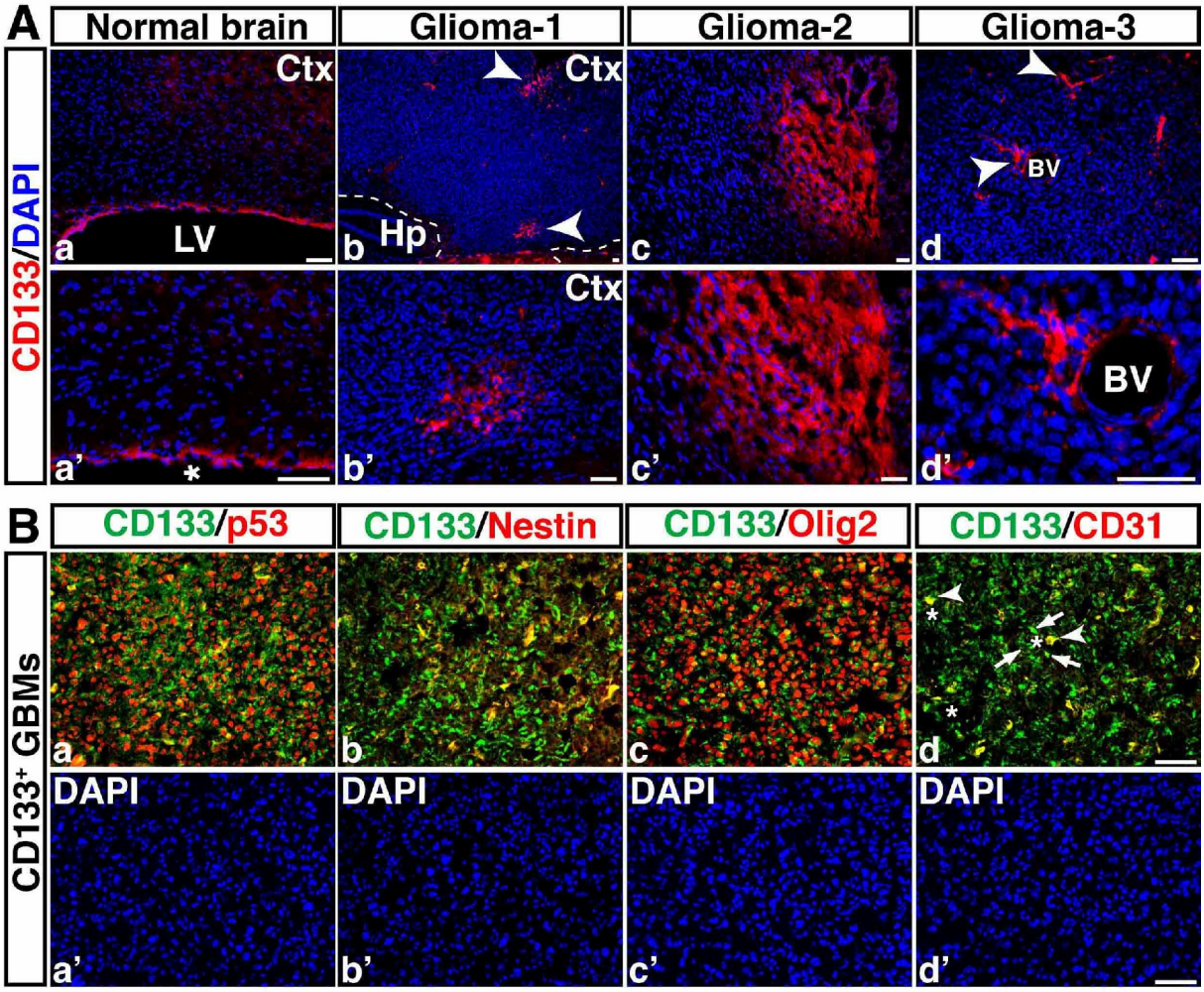

Supplemental Figure 5

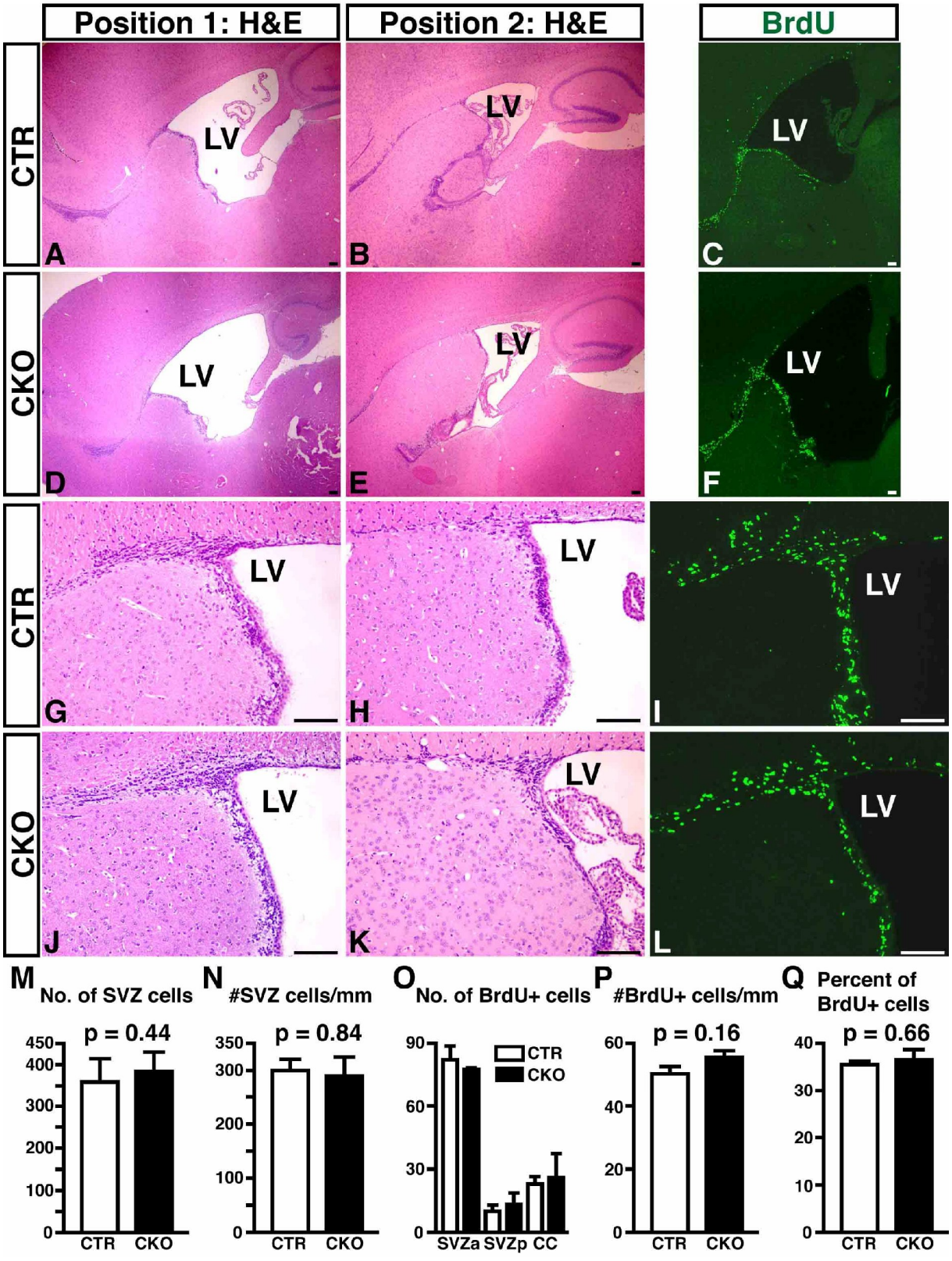

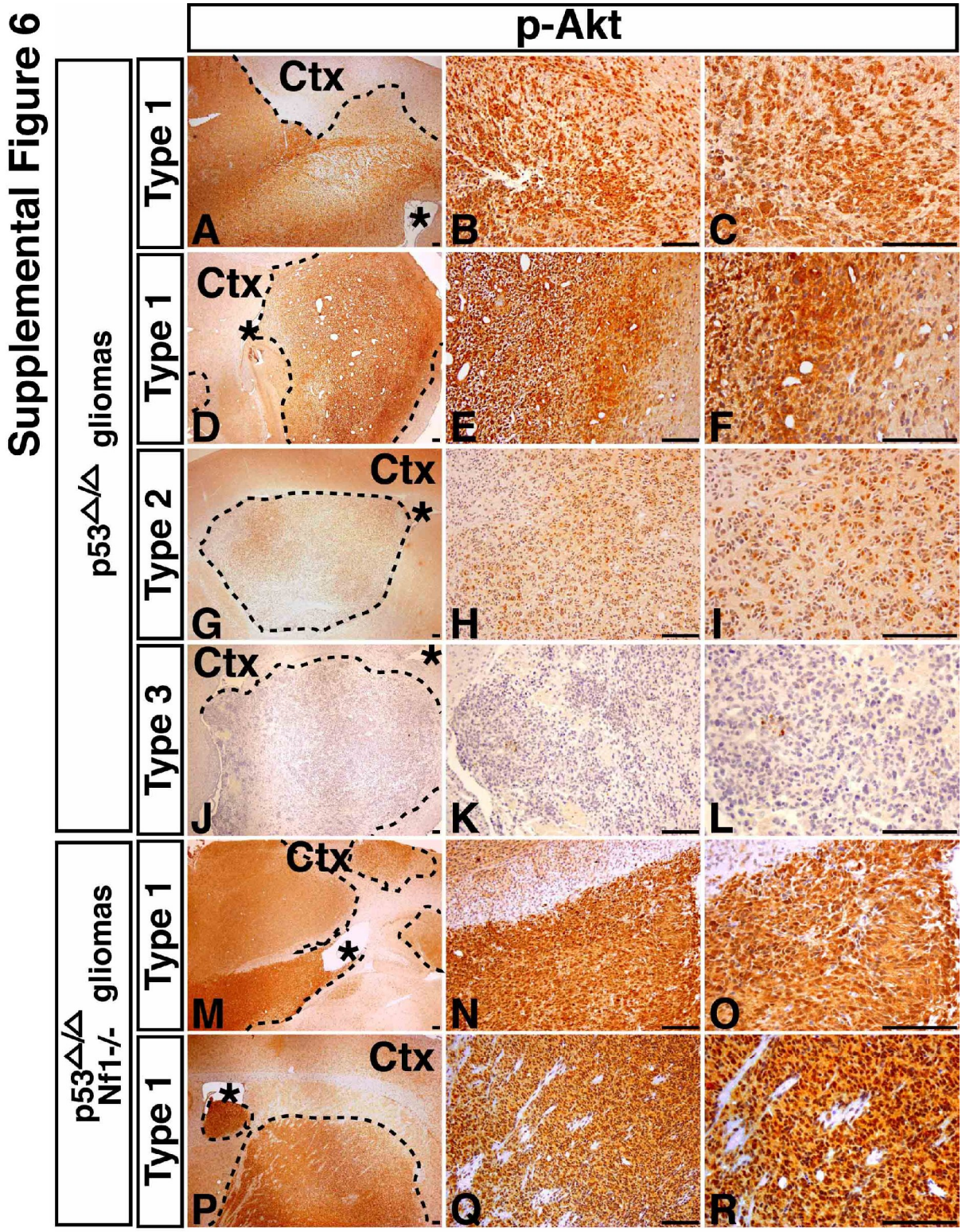
Supplemental Figure 6
p-Akt
p53Δ/Δ gliomas
p53Δ/Δ Nf1-/- gliomas
Type 1
Type 1
Type 2
Type 3
Type 1
Type 1
Ctx
A
B
C
D
E
F
G
H
I
J
K
L
M
N
O
P
Q
R

Supplemental Figure 7

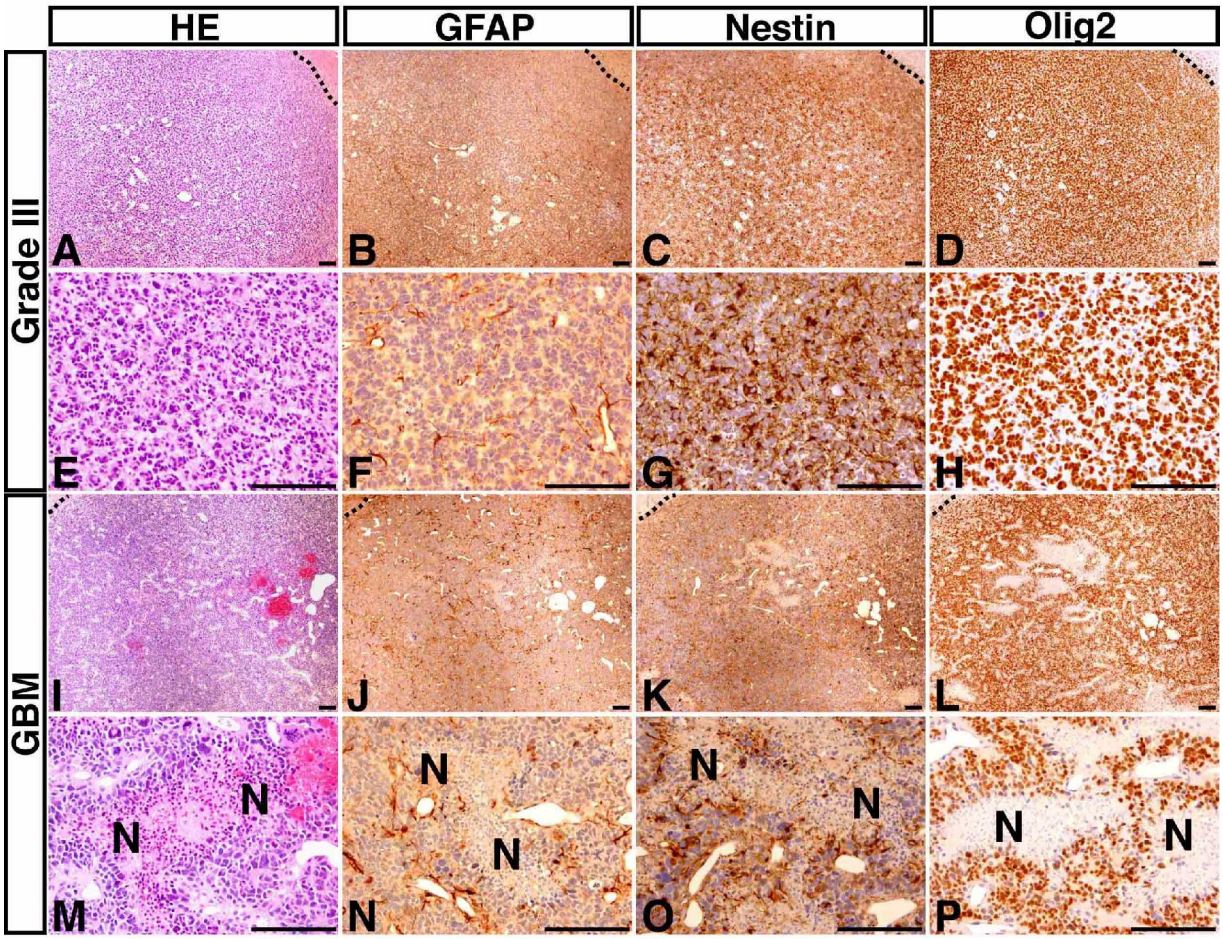

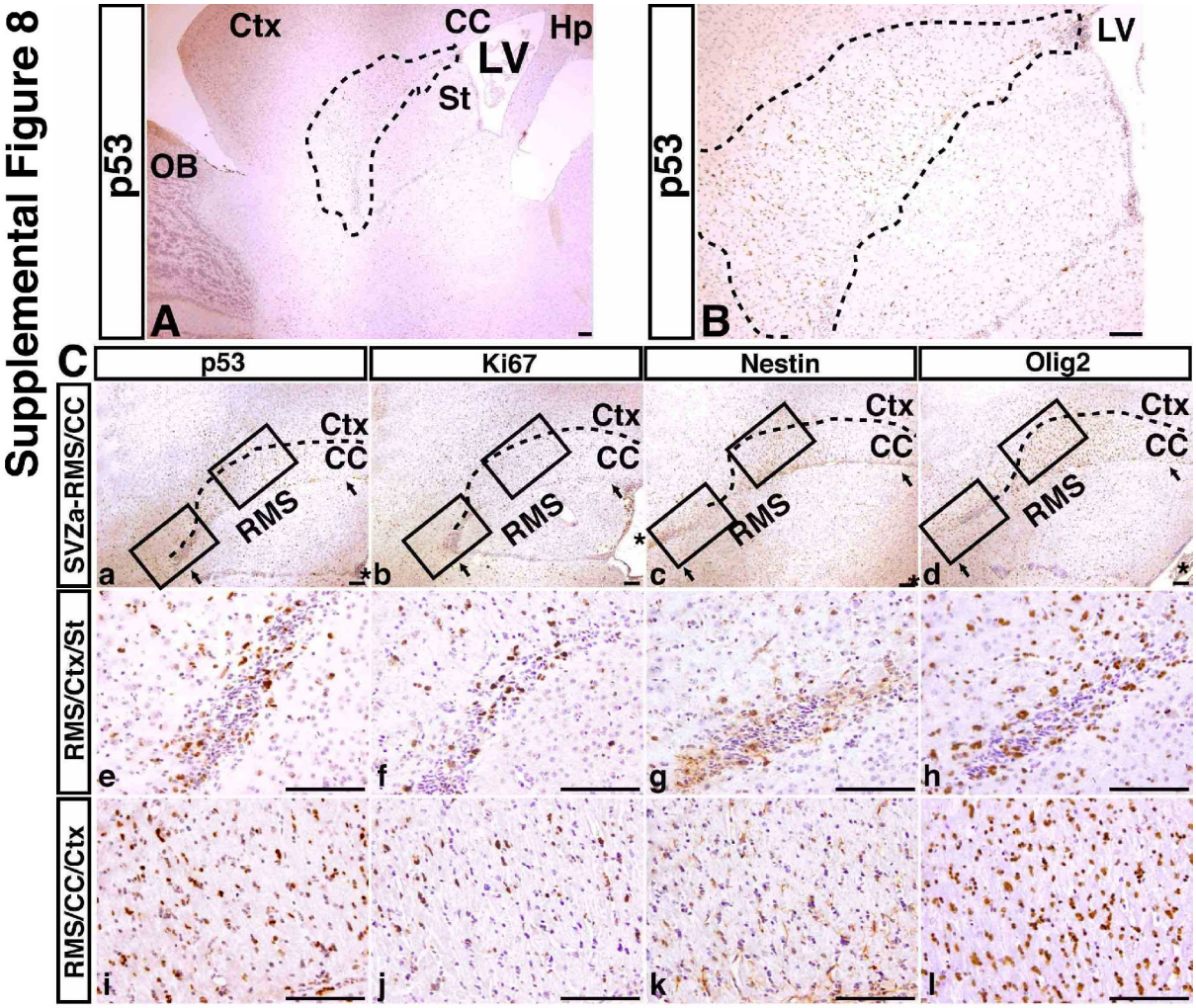
Supplemental Figure 8
p53
Ctx
CC
Hp
LV
St
OB
A
p53
LV
B
C
p53
Ki67
Nestin
Olig2
SVZa-RMS/CC
RMS/Ctx/St
RMS/CC/Ctx
Ctx
CC
RMS
a
b
c
d
e
f
g
h
i
j
k
l

Supplemental Figure 9

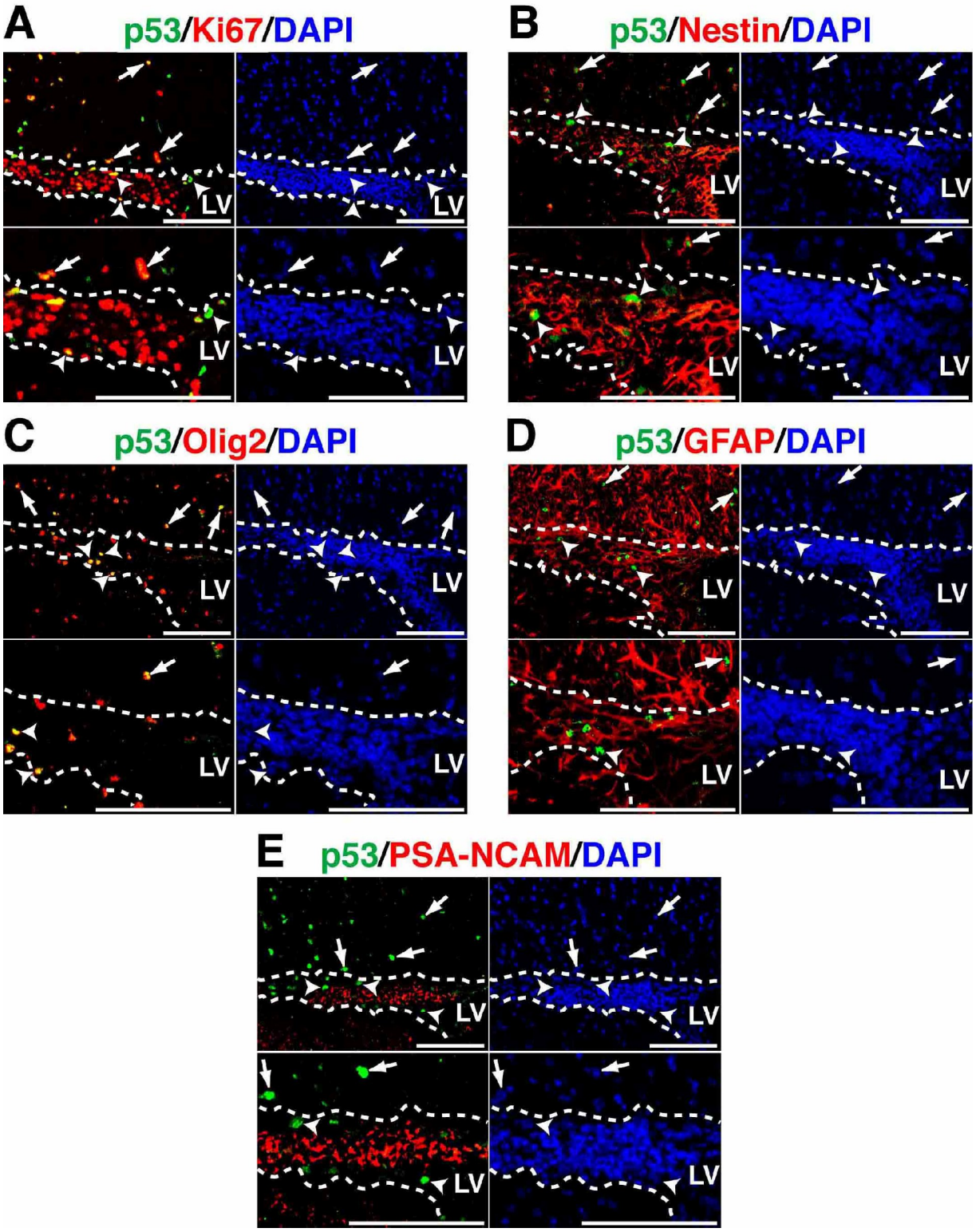

Table S1. Negative controls for p53 immunohistochemical analysis

Mouse genotype	No. Mice	p53 IHC
hGFAP-cre-;$p53^{flox/KO}$	n = 1	Negative
hGFAP-cre-;$p53^{flox/flox}$	n = 4	Negative
hGFAP-cre-;$p53^{flox/flox}$;$Nf1^{KO/+}$	n = 4	Negative
hGFAP-cre+;$p53^{flox/+}$	n = 10	Negative
hGFAP-cre+;$p53^{KO/KO}$;$Nf1^{flox/flox}$	n = 3	Negative
hGFAP-cre+;$p53^{KO/+}$;$Nf1^{flox/+}$	n = 2	Negative

Table S2. Summary of immunohistochemical analysis of malignant astrocytic gliomas

CKO1	n = 10					
Mouse I.D.	**Brain I.D.**	**Grade**	**Nestin**	**GFAP**	**Oligo2**	**p-Erk**
040309,#1	Y160	Grade III	++++	LMD	+++++	+
040403, #2	Y163	Grade III	+++++	+	+++++	-
040405, #1	Y164	Grade III	+++	**++**	+++++	+ & ++
040609, #10	Y321	Grade III	++ & +++	+	+++++	+
041126, #1	Y452	Grade IV	+++++	+++	++++	++
041201,#1	Y475	Grade IV	++ & ++++	++	N.D.	+
050212,#4	Y480	Grade IV	++	+++	+++++	++
050228,#2	Y504	Grade IV	+++ & ++++	+	+++++	+
050524,#1	Y577	Grade III	+++	+++	+++++	+++
050510,#3	Y551	Grade III	+++	N.D.	+++++	N.D.

CKO2	n = 10					
Mouse I.D.	**Brain I.D.**	**Grade**	**Nestin**	**GFAP**	**Oligo2**	**p-Erk**
040216,#1	Y81	Grade III	++++	LMD & focal	N.D.	+
040923,#1	Y327	Grade IV	++ & +++++	++	++++	++
041115,#1	Y347	Grade III	+++	LMD	+++++	++
041228,#3	Y489	Grade IV	+++++	+	+++++	-
050103,#1	Y506	Grade IV	++	++	++++	++
050123,#1	Y483	Grade IV	+ & ++	+ & +++	- & ++++	++ & +++
050211,#2	Y485	Grade IV	-	+++	++ & ++++	-
050716,#5	Y693	Grade III	+ & ++ & ++++	++++	++++ & +++++	+ & ++
050720,#2	Y696	Grade III	++++	+++	+++++	- & +++
050510,#4	Y544	Grade III	++++	N.D.	+++++	N.D.

CKO3	n = 15					
Mouse I.D.	**Brain I.D.**	**Grade**	**Nestin**	**GFAP**	**Oligo2**	**p-Erk**
030709,#5	Y25	Grade IV	+++++	LMD & focal	N.D.	++ & ++++
030711,#1	Y26	Grade III	+++++	LMD & focal	N.D.	++++
041023,#1	Y344	Grade IV	+++++	LMD	+++++	++
041122,#8	Y492	Grade IV	+++++	LMD	N.D.	+++
041130,#4	Y494	Grade IV	+++	LMD	+++++	++++
050228,#3	Y507	Grade IV	+++++	LMD	N.D.	++++
050525,#3	Y580	Grade III	+++++	LMD	N.D.	++++

050525,#4	Y582	Grade IV	+++++	LMD	+++++	++++
050601,#5	Y654	Grade III	+++++	LMD	+++++	++++
050612,#2	Y656	Grade IV	+++++	LMD	N.D.	+++
050708,#2	Y658	Grade IV	+++++	LMD	+++++	++
050708,#3	Y660	Grade IV	+++++	LMD	+++++	+++
050708,#5	Y662	Grade IV	+++++	LMD & focal	+++++	+++
050716,#3	Y664	Grade IV	+++++	-	+++++	+
050510,#5	Y553	Grade III	+++++	LMD	+++++	N.D.

LMD, low or moderate level of diffusive staining. N.D., Not determined

Grading criteria:

-	Negative
+	1 to 5%
++	6 to 20%
+++	21 to 40%
++++	41 to 80%
+++++	> 80%

p-Akt
++++
+
++ & +++
- & ++
++++
++++
++++
+++++
++++
N.D.

p-Akt
++++
++++
++++
++++
++++
+ & +++
++++
++++
++++
N.D.

p-Akt
++++
+++ & ++++
N.D.
+++++
+++++
+++++
++++

+++++
++++
+++++
++++
+++++
+++ & ++++
+++++
N.D.

Table S3. The location and number of p53-positive cells

Mouse Number	Forebrain		
	SVZa/RMS/CC	SVZ/CC/Ctx	Other
1	S1	S2	N
2	N	S1	N
3	S1	S1	S1
4	S1	S2	N
5	S1	S2	N
6	S1	N	N
7	S2	S2	S1
8	S2	S2	N
9	S1	S2	N
10	ND	S2	N
11	ND	S3	N
12	S1	S2	N
13	S1	S1	N
14	S1	S1	N
Total	11/12	13/14	2/14